Journal of Non-Crystalline Solids 435 (2016) 8–16

Contents lists available at ScienceDirect

Journal of Non-Crystalline Solids

journal homepage: www.elsevier.com/locate/jnoncrysol

Peroxo method for preparation of composite silica–titania spheres

Roman Morozov [a], Igor Krivtsov [a,b,*], Viacheslav Avdin [a], Zakariae Amghouz [c], Sergey A. Khainakov [c], José R. García [b]

[a] Department of Chemistry, South Ural State University, 454080 Chelyabinsk, Russia
[b] Department of Organic and Inorganic Chemistry, University of Oviedo-CINN, 33006 Oviedo, Spain
[c] Scientific-Technical Services, University of Oviedo, 33006 Oviedo, Spain

ARTICLE INFO

Article history:
Received 30 October 2015
Received in revised form 27 December 2015
Accepted 30 December 2015
Available online xxxx

Keywords:
Silica–titania
Spherical particles
Stober process
Titanium peroxo complex

ABSTRACT

Composite silica–titania spherical particles, from the nanometer to submicron size, have been synthesized *via* a new template-free method, being achieved by the reaction of aqueous titanium peroxo complex with TEOS (tetraethylorthosilicate) in aliphatic alcohols. The choice of the solvent greatly affects the growth of silica–titania particles. It has been established that size of the spheres increases as carbon chain length of alcohol extends (from methanol to n-propanol). The nanometer size SiO_2–TiO_2 spheres with mean diameter of about 50 nm are formed in the methanol solution, while n-propanol promotes particle growth up to 400 nm. The synthesized composites retain amorphous structure up to 500 °C due to the formation of Si–O–Ti heterolinkages, whose presence has been confirmed by FTIR and XPS studies.

1. Introduction

Titania is well-known for its unique catalytic properties, low toxicity, chemical stability and availability. Unsurprisingly, a large number of reviews, devoted to fundamental aspects of TiO_2 as well as its industrial applications, have recently been published [1–5]. Also, titania-based composites attract a considerable attention no less than pure TiO_2 [6], as they tend to enhance its performance in photocatalytic reactions, photovoltaic devices [7], dye-sensitized solar cells [8] and olefine epoxidation catalysis [9]. Among the mixed TiO_2–M_xO_y oxides, TiO_2–SiO_2 acquired a special interest of the researchers [10–15]. The tunability and flexibility of silica–titania properties favor formation of a wide range of functional materials. Preparing mixed oxides with core–shell structure, *via* modification of silica particles with titania molecular or sol precursor [16,17] or covering TiO_2 with SiO_2 layer [18,19], can serve well for various applications but primarily for photocatalysis, because the thin layer of SiO_2 on crystalline anatase particles enhances adsorptive properties and facilitates light-assisted degradation of water pollutants [20–22]. Contrary to photocatalysis, which demands crystalline TiO_2, acid catalysis prefers amorphous material with high dispersion of active sites. Isomorphous substitution of Si^{4+} by titanium cations in the silica matrix, tends to reduce the coordination number of some titanium atoms to the 4-coordinated state, and therefore hinders the crystallization process of TiO_2 due to its dispersion in silica and the formation of Si–O–Ti bonds [11,23]. The presence of Si–O–Ti heterolinkages is vital for the reactions catalyzed by silica–titania materials [24–26], however, some other important properties of silica such as high chemical stability and surface area also promote the catalytic performance of the mixed oxide [27]. There are many ways to produce SiO_2–TiO_2 composite materials with different degrees of molecular homogeneity; among them are the following: sol–gel processing [28–31], solvothermal synthesis [32,33], and electro-spinning methods [34]. Moreover, by changing the synthetic conditions one can tune morphology of silica–titania and obtain fibers [34], bulk porous material [29], or spherical particles [35]. Spheres of nanometer to micrometer sizes are of special interest for application in chromatography columns and catalytic reactors, because they could provide dense packing and regular flow of a mobile phase or a reactant [36–40]. The submicron- and micron-sized spherical particles – unlike nanoparticles – are easily separable from the reaction media, which could be beneficial for their application as catalyst supports and other purposes [41,42]. Many researchers target the preparation of mesoporous spherical silica particles aiming to utilize them as catalyst supports, but nonporous material of the same spherical morphology is of no less interest. It has been demonstrated that application of nonporous SiO_2 as a catalytic support and for drug delivery purposes has its benefits [43,44]. It facilitates mass transport in the reaction bed, and high degree of hydroxylation provides adsorption sites enabling anchoring of certain molecules, even despite the low surface area of the material [45]. However, morphology control is not the only problem one encounters while dealing with SiO_2–TiO_2 composites. The formation of homogeneous silica–titania spherical composites is not an easy task, since silicon and titanium have very different hydrolysis rates, therefore, in order to equalize them complexing agents or pre-hydrolysis of silica precursors

* Corresponding author.
E-mail addresses: uo247495@uniovi.es, zapasoul@gmail.com (I. Krivtsov).

http://dx.doi.org/10.1016/j.jnoncrysol.2015.12.024
0022-3093/

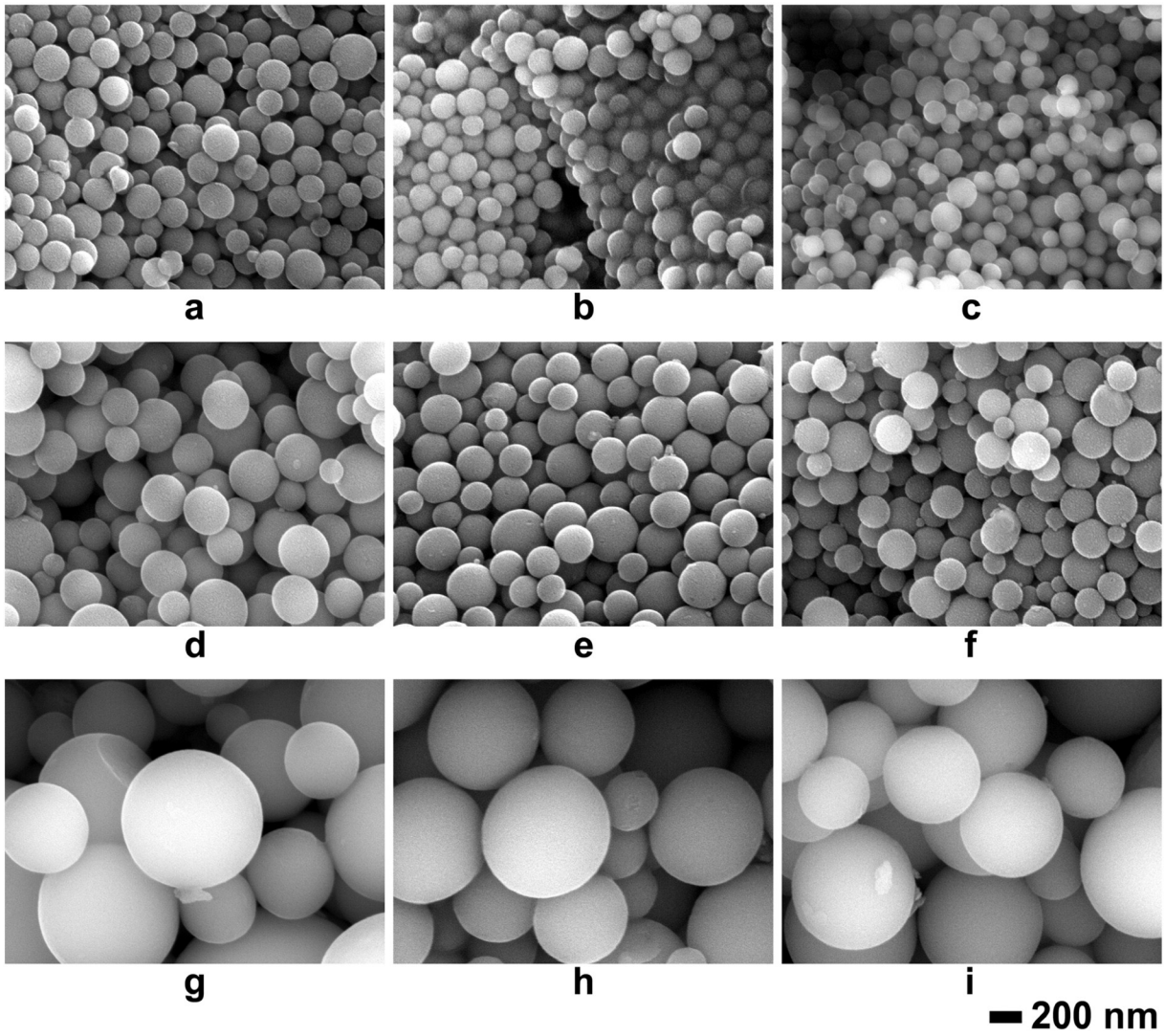

Fig. 1. SEM-images of samples (a–c) Me-as, Me-500 and Me-1000; (d–f) Et-as; Et-500; Et-1000; (i–k) Pr-as, Pr-500, Pr-1000.

are usually applied [11]. The high reactivity of titania precursors in water media drives researchers to use titanium alkoxides in organic solvents instead of its inorganic salts, so that the hydrolysis rate is controlled more efficiently [46–48]. However, the replacement of unstable and toxic titanium alkoxides by stable water-soluble titania precursors is a desired goal. The preparation of silica–titania materials using aqueous titanium peroxo complexes *via* sol–gel and hydrothermal methods was previously described by our research group [22,49], but the resulting materials appeared to be segregated. The goal of the present study is to describe a new preparation procedure of thermally stable silica–titania nanometer- and submicron-sized nonporous spherical particles with high degree of molecular mixing *via* the peroxo-mediated Stober-like process. The proposed procedure allows formation of the mentioned composites with the mean sizes varying from 50 to 400 nm, depending on the choice of solvent. The silica–titania spheres stay amorphous up to 500 °C due to the presence of Si–O–Ti linkages in their structure.

Table 1
The values of surface area and pore volume of the silica–titania samples.

	BET surface area, m^2/g	BJH desorption pore volume, cm^3/g
Me_150	28	0.17
Et_150	28	0.18
Et_150	27	0.04
Me_500	19	0.17
Et_500	19	0.18
Pr_500	5	0.02
Me_700	18	0.17
Et_700	23	0.19
Pr_700	8	0.03

2. Experimental

2.1. Chemicals

TEOS was purchased from Aldrich and used as silica source. Titanium oxysulfate hydrate ($TiOSO_4 \cdot H_2O$) containing not more than 17% of H_2SO_4 was produced by Alfa Aesar. Ammonia 25 wt% water solution ($NH_3 \cdot H_2O$) and 30 wt% aqueous hydrogen peroxide solution were provided by VWR Chemicals.

2.2. Synthesis of the composite silica–titania spheres

A combined procedure based on Stober process [50] and the solvent-exchange method, described earlier for TiO_2 nanoparticles preparation [51], was implemented for the synthesis of the silica–titania spheres. The first step of the synthesis was the preparation of a peroxotitanate complex solution. For this purpose 2.5 mmol of titanium oxysulfate

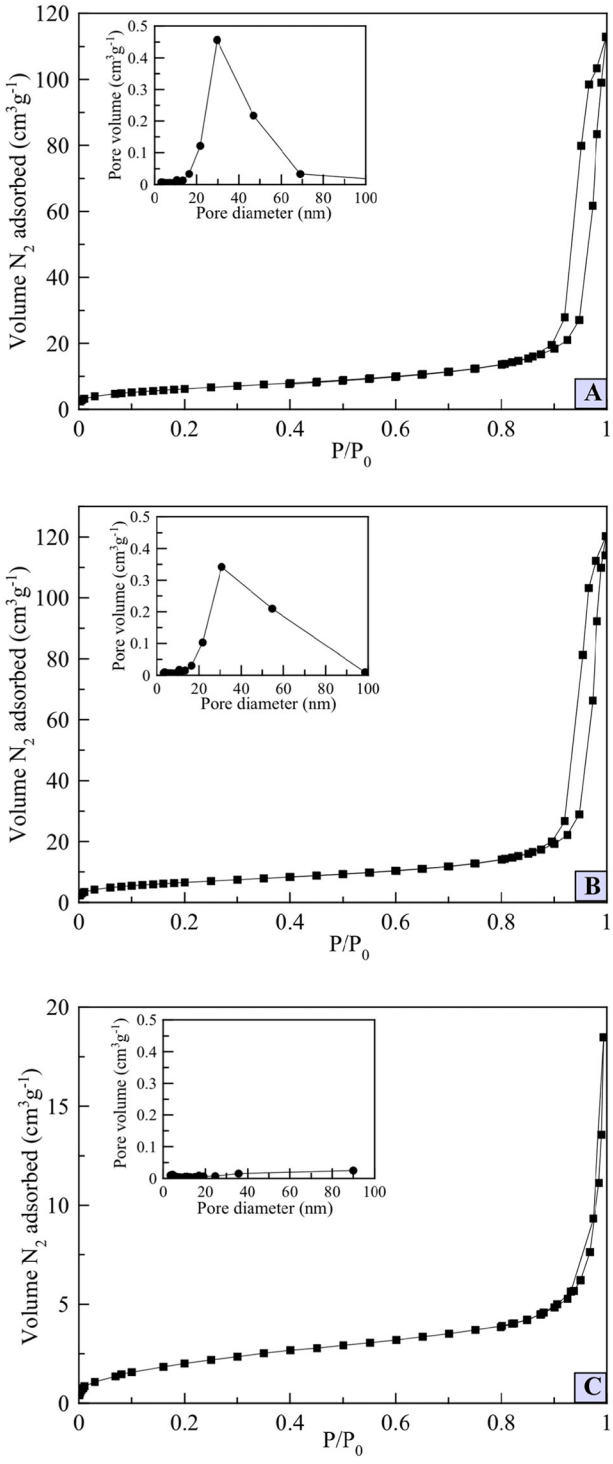

Fig. 2. N_2/77 K adsorption–desorption isotherms of (A) Me-500, (B) Et-500, and (C) Pr-500 samples.

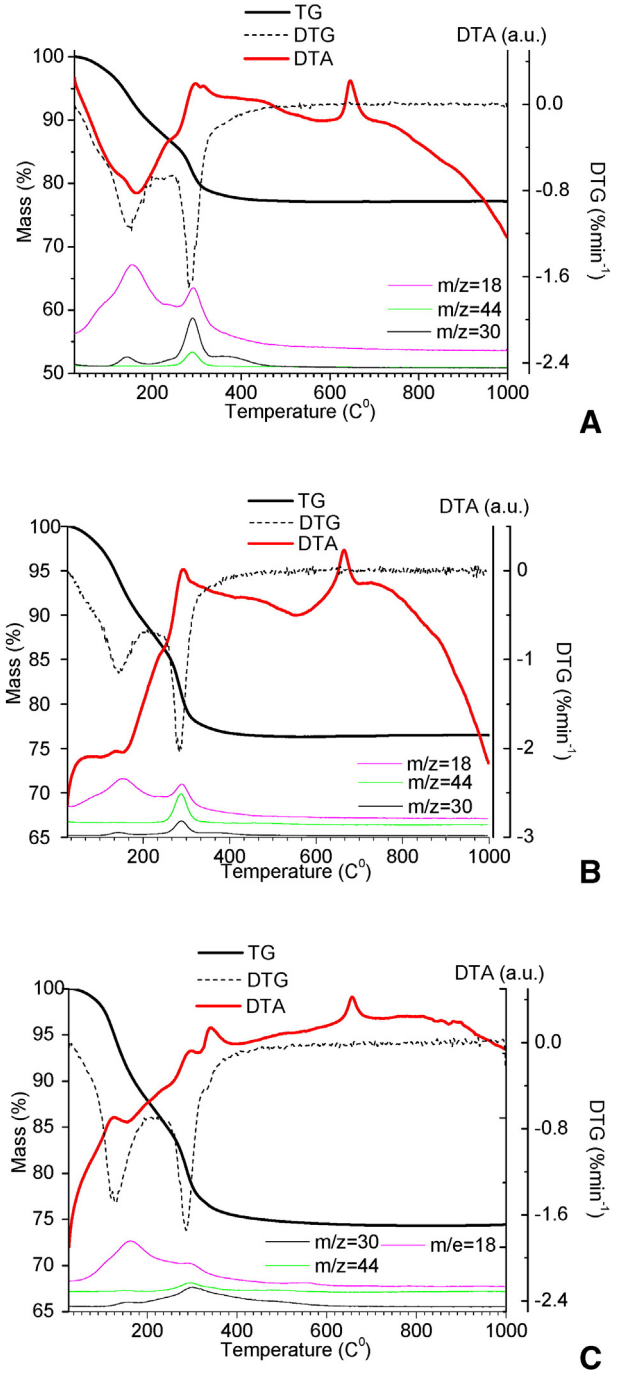

Fig. 3. Thermoanalytical curves and corresponding EGA of (a) Me-as, (b) Et-as, and (c) Pr-as samples.

was dissolved in deionized water under heating at 50 °C. When the solution became clear, 2.5 mL of ammonium hydroxide was added causing precipitation of colloidal titanium hydroxide. The precipitate was centrifuged at 7000 rpm and washed 6 times with deionized water. Then 2.5 mL of hydrogen peroxide was added to the washed titanium hydroxide and thoroughly stirred until the transparent orange solution of peroxotitanate complex appeared. Then, its pH value was adjusted to 9.5 by addition of 3 M ammonium hydroxide solution. Finally, the obtained solution of the peroxotitanate complex was diluted to 25 mL with deionized water. Separately, 25 mL of a solution containing 2.5 mmol of TEOS in an alcohol (methanol, ethanol, or n-propanol) was prepared. Under vigorous stirring, the peroxotitanate complex solution was poured into the TEOS solution, as a result the turbid yellow-colored suspension is formed immediately. After 24 h of stirring, the suspension was centrifuged at 7000 rpm, washed 6 times with deionized water and dried under vacuum at 50 °C. After that, the samples were thermally treated in a muffle furnace at 500 °C, 700 °C, and 1000 °C with a heating rate of 3 °C min^{-1} and calcination time of 1 h. The reproducibility of the whole procedure was ensured by the preparation of at least three replicates of each type of sample. The samples are designated in the following way: S-*x*, where S is the solvent used for the synthesis

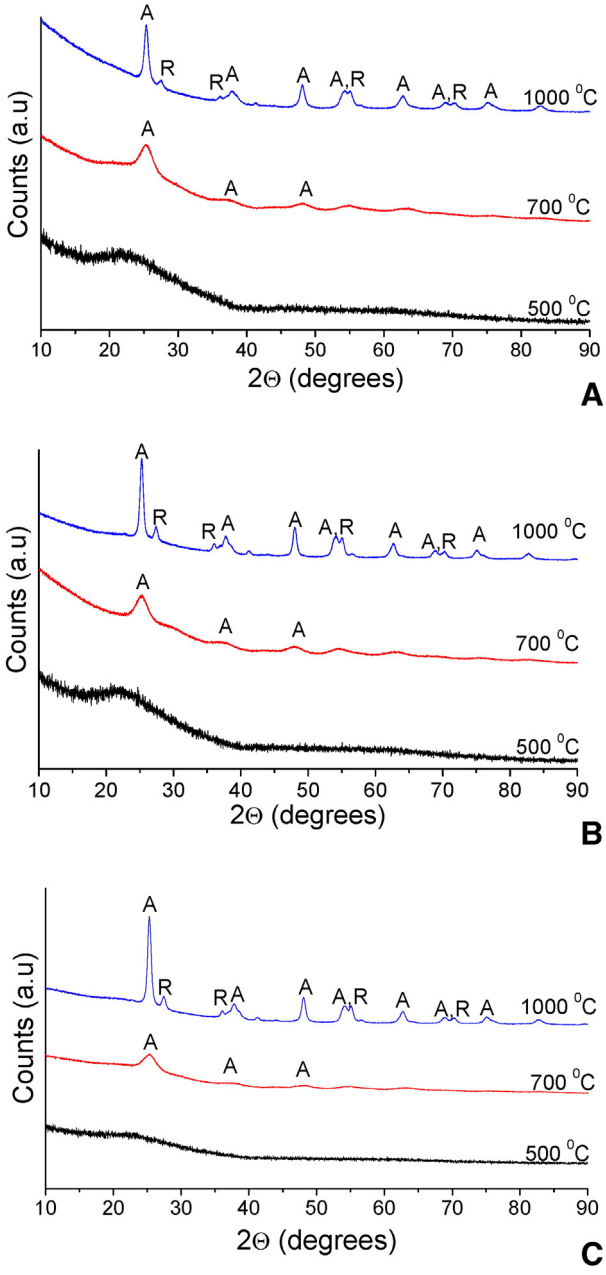

Fig. 4. Powder XRD patterns of the samples calcined at certain temperatures: (a) Me, (b) Et, (c) Pr.

(Me is for methanol, Et for ethanol, and Pr for n-propanol) and *x* stands for the heat treatment temperature, while *as* means as-prepared.

2.3. Characterization

Morphology and elemental composition of the prepared materials were investigated using a field emission scanning electron microscope (SEM) Jeol JSM 7001F equipped with Oxford Instruments elemental EDS analyzer. Nitrogen physisorption at 77 K was measured by an ASAP Micromeritics 2020 instrument. The samples were outgassed at 250 °C under vacuum prior to analysis. X-ray diffraction (XRD) patterns were recorded by a Rigaku Ultima IV diffractometer operating at Cu-Kα radiation (λ = 0.154 nm). Sizes of anatase and rutile crystals were calculated from XRD data by applying Scherrer equation. The mass ratio of anatase to rutile in the calcined samples was established using Spurr Eq. (1).

Table 2
Crystallite sizes and rutile phase content of the samples.

Sample	Anatase crystal size, nm	Rutile crystal size, nm	Rutile content, wt%
Me-700	4	–	0
Et-700	7	–	0
Pr-700	3	–	0
Me-1000	12	15	4.7
Et-1000	15	15	19.1
Pr-1000	14	14	16.8

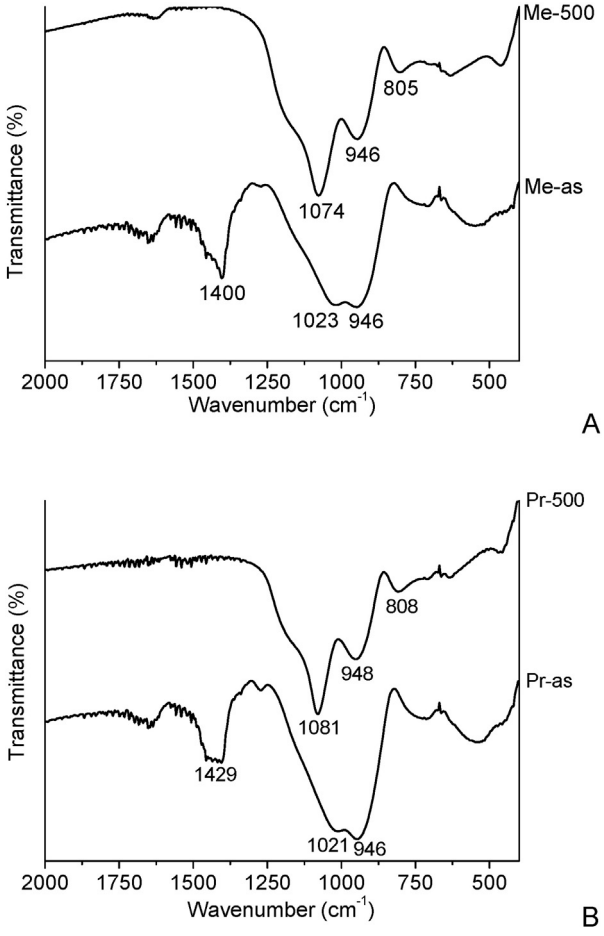

Fig. 5. FTIR spectra of (a) Me and (b) Pr samples.

$$F_R = \frac{1}{1 + 0.8[I_A(101)/I_R(110)]} \times 100 \quad (1)$$

where, F_R is the fraction of rutile; I_A is the integrated intensity of anatase peak (101); I_R is the integrated intensity of rutile peak (110).

Thermoanalytical study and evolved gas analysis (EGA) were carried out by a simultaneous thermal analyzer Netzsch Jupiter 449C, coupled with Aeolos QMS 403C mass-spectrometer, in the range from 25 °C to 1000 °C in air, with the heating rate of 10 °C·min^{-1}. Infrared spectra were recorded from the samples powdered and pressed in KBr pellets using a Brucker Tensor 27 spectrometer. X-ray Photoelectron Spectroscopy (XPS) analysis was carried out using a SPECS system equipped with a Hemispherical Phoibos detector operating in a constant pass energy, using Mg-Kα radiation (h · υ = 1253.6 eV). Transmission electron microscopy (TEM) studies were performed on a JEOL JEM-2100F transmission electron microscope operated at an accelerating voltage of 200 kV, equipped with a field emission gun (FEG) and an ultra-high resolution pole-piece that provided a point-resolution better than 0.19 nm. The samples for TEM were dispersed in ethanol, sonified and

sprayed on a holey carbon film coated copper grid, then allowed to air–dry; finally, Gatan SOLARUS 950 was used before observation.

3. Results and discussion

3.1. Morphology and N_2 physisorption

First of all, the prepared silica–titania samples have been investigated by SEM-EDS technique aiming to determine their morphological characteristics, particle sizes, and elemental composition. Fig. 1 shows that our suggested synthetic procedure leads to the formation of spherical particles having a smooth surface, regardless of the solvent used for their synthesis. One might notice that sizes of the spheres are not the same for different samples. The smallest particles are formed in methanol solution (Fig. 1a–b), while n-propanol favors particle growth (Fig. 1g–i). Thus, increase of the size of the spheres is attributed to increased length of the carbon chain of an alcohol. While, heat treatment does not have any significant effect on the morphological properties of the spheres (Fig. 1). The analysis of elemental composition by EDS shows that the Si:Ti molar composition is close to equimolar.

Specific surface area of the silica–titania samples decreases as the carbon chain length of the used solvent increases. This result is in accordance with SEM observations, demonstrating a significant particle growth when changing the solvent in the following sequence methanol–ethanol–propanol (Table 1). Fig. 2 shows the most representative data of N_2 physisorption. One can note that all samples display IV-type isotherm with H1-type hysteresis loop according to IUPAC classification, which indicates the presence of large mesopores (Table 1). According to the pore size distribution of Me-500 and Et-500 samples (Fig. 2a,b), they contain mesopores with a mean diameter of 40–50 nm, which is comparable with their particle sizes. The hysteresis loop, clearly observed for Me-500 and Et-500 samples, is barely distinguishable on the adsorption–desorption isotherm of Pr-500 (Fig. 2c). The pore size distribution analysis of this sample suggests its nonporous nature. The nonporous character of the prepared oxides is evidently the consequence of the synthetic procedure, as the samples calcined at 150 °C possess very similar adsorption–desorption profiles (Supplementary Information Fig.S1). Increase of the calcination temperature up to 700 °C does not affect the porosity of the silica–titania spheres to a great extent, as no significant changes in the values of surface area or adsorption–desorption profiles are observed (Fig. S2, Table 1). Considering these very low surface area values and isotherms profiles one might conclude that prepared spherical composites are nonporous, and it is reasonable to assign the mesopores of the silica–titania samples to the interparticle voids rather than internal porosity.

3.2. Thermoanalytical study

The as-prepared samples formed at near room-temperature conditions, so, they expected to contain physically and chemically adsorbed water, unreacted species and reaction by-products, and also they might undergo certain thermally induced polymorphic transformations. Thermogravimetry (TG) curves (Fig. 3) show the total mass loss in the range of 23–26% for all samples. The loss of volatile compounds from the silica–titania composites is accomplished in two well-defined stages, which can be distinguished on the DTG curves.

The corresponding mass spectrometric (MS) signals indicate that the product with m/z 18, which is most likely to be physically adsorbed and chemically bonded water, is evacuated in the first stage below

Table 3
XPS surface elemental composition.

Sample/atoms	O, at%	Ti, at%	Si, at%
Me-500	57.0	6.0	37.0
Pr-500	56.0	8.1	35.9

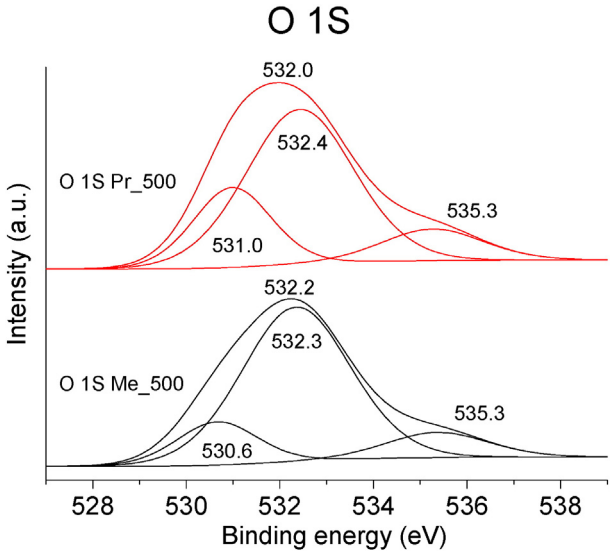

Fig. 6. XPS O1s spectra of Me-500 and Pr-500 samples.

200 °C. In the following stage, the oxidation of organic residue and ammonia bonded to the composite takes place. The exothermic nature of this process is evident from the differential thermal analysis (DTA) curves (Fig. 3). It results in the appearance of m/z44 and 30 signals, which are assigned to CO_2 and NO respectively, and it is also accompanied by water removal. The decomposition step is terminated at about 350 °C. However, one can observe the exothermic effect on the DTA curves in the range of 600–700 °C, as no mass loss is seen at these temperatures, the peak should be assigned to a phase transition of titania.

3.3. XRD analysis

In order to assign the thermal effects observed on the thermoanalytical curves, the samples have been calcined at certain temperatures in a muffle furnace according to TG/DTA data. The as-prepared samples are amorphous, as well as those thermally treated up to 500 °C (Fig. 4). The effect observed on the DTA curves in the range of 600–700 °C is undoubtedly attributed to the transformation of amorphous titania to crystalline anatase phase. After crystallization process, small titania anatase crystals are formed; a mean size of the crystals has been calculated using Scherrer equation (Table 2). Further heat treatment results in enhancing the crystallinity of TiO_2 contained in the composites and its partial transition into the thermodynamically stable rutile phase. The content of the rutile phase has been calculated using Spurr equation, and it appears that the anatase-to-rutile phase transformation is more favorable in larger silica–titania particles (Table 2).

3.4. Spectroscopic study

The ability of the prepared samples to remain amorphous up to relatively high temperatures indicates the incorporation of Ti^{4+} into silica matrix by forming Si–O–Ti heterolinkages. These bonds are of great importance in materials of this type, since they provide formation of catalytically active sites [24–26].

In order to gain a deeper understanding of the structural features of the amorphous composites spectroscopic studies have been performed. The samples having the smallest and the largest particle sizes, *e.g.* Me and Pr ones, have been selected for investigation. FTIR study shows the presence of bonded ammonia in the as-prepared composites, which is indicated by the band at 1400–1430 cm^{-1} (Fig. 5a,b). This band is no longer present in the spectra of the thermally treated

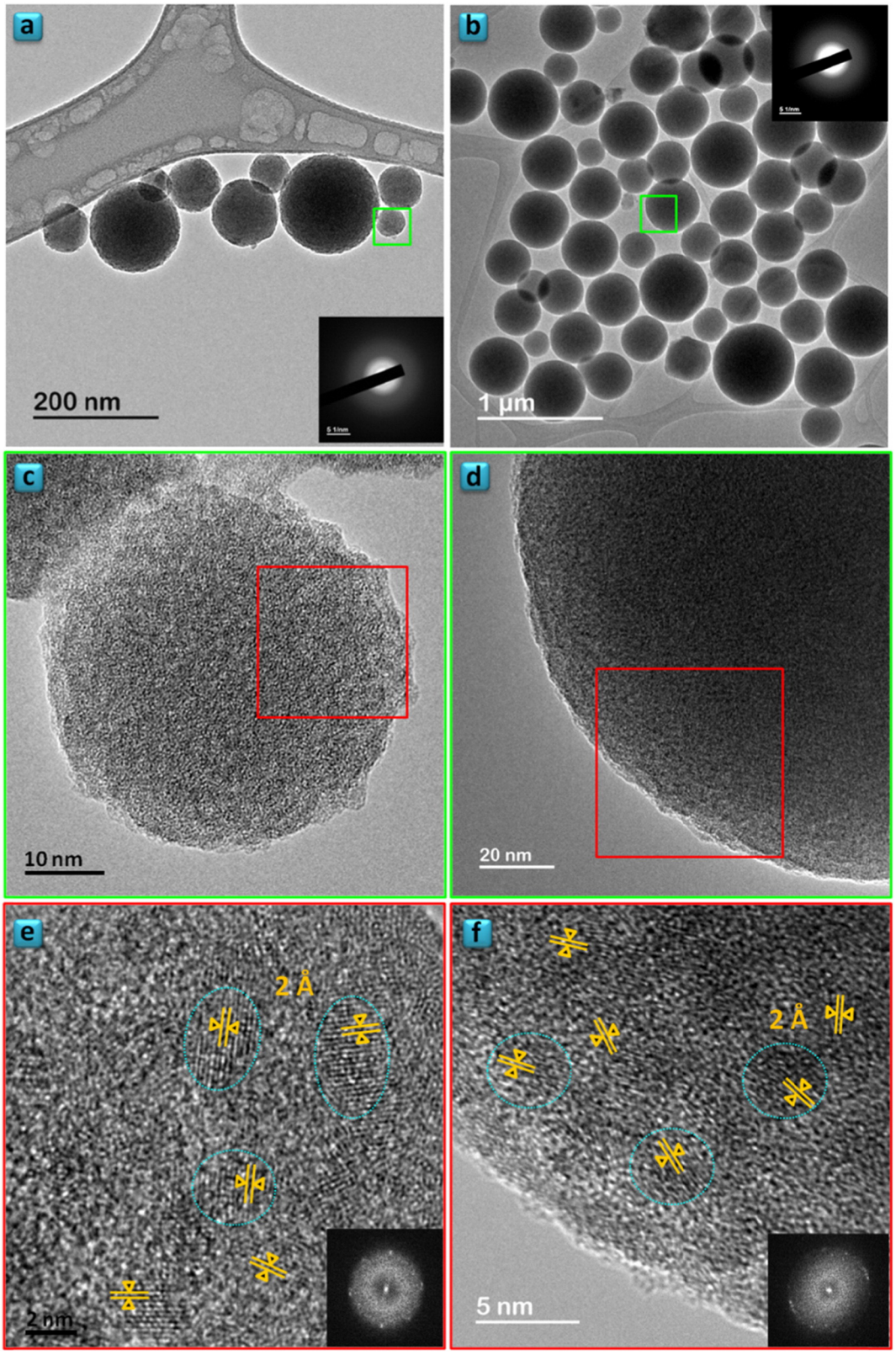

Fig. 7. TEM images of Me-500 (a,c) and Pr-500 (b,d); the insets show elected area electron diffraction (SAED) patterns; (c,d) correspond to magnification of the zone highlighted by the green square in (a,b). HRTEM images of Me-500 (e) and Pr-500 (f) of the zone highlighted by the red square in (c,d); the insets show FFT, the interplanar distances are marked with yellow bars, and the blue dashed circles show the size of the crystallites. (For interpretation of the references to color in this figure legend, the reader is referred to the web version of this article.)

samples, where ammonia decomposition has also been observed on the TG/DTA-MS data. The most valuable information provided by FTIR spectra concerns the bonding between silica and titania species in the composite oxides. Earlier [11], we applied this technique to characterize silica–titania materials prepared *via* the aqueous peroxo method, where we established that the formation of SiO_2–TiO_2 oxides was as a segregated pure silica and titania. However, the opposite is observed in the present case, which makes the peroxo-mediated procedures

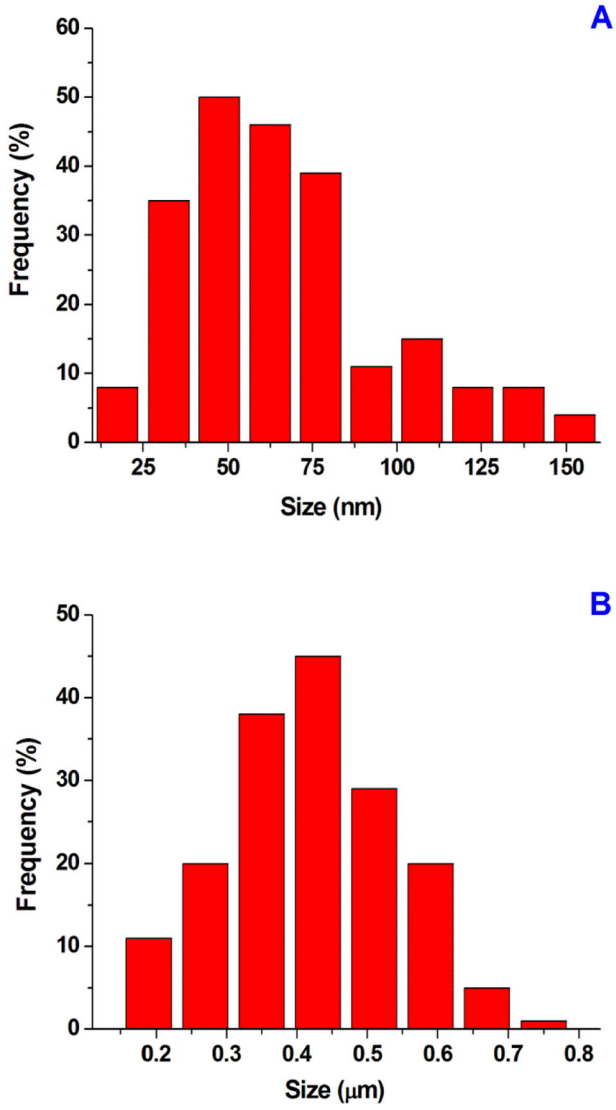

Fig. 8. Histograms of particle size distribution for Me-500 (a) and Pr-500 (b).

flexible in terms of governing the local structure of the material. Silica usually shows absorption in the range of 1250–1070 cm^{-1}, which corresponds to the asymmetric stretching vibrations of Si–O–Si bonds. This band has a tendency to shift toward lower wavenumbers, when a fraction of silicon atoms is replaced by other metals [11]. This shift is significant in the spectra of the as-prepared composites, where the band has a maximum around 1021–1023 cm^{-1} (Fig. 5). The incorporation of Ti^{4+} into silica network is also confirmed by the appearance of a band near 950 cm^{-1} [11], the peak in this region (centered at 946 cm^{-1}) has a high intensity on the spectra of both as-prepared samples. Thermal treatment at 500 °C results in some obvious changes in the structure of the composites. The band corresponding to the υ_{as}(Si–O–Si) is shifted to 1074 and 1081 cm^{-1}, which is likely to be the consequence of partial segregation of the two oxides. The band assigned to Si–O–Ti remains in the same position like the samples before being calcined, though its intensity is decreased in relation to the υ_{as}(Si–O–Si) peak. The most explicit indication regarding the partial separation of silica from the composite is the appearance of the low-intensity peak at 805 and 808 cm^{-1} in the spectra of Me-500 and Pr-500 samples, assigned to the symmetric stretching of Si–O–Si bonds [52]. This means that some amount of the silica, not distorted by the incorporation of Ti^{4+}, is formed after thermal treatment allowing us to observe the υ_{sm}(Si–O–Si) in the spectra. Even though the Si–O–Ti bonds are still present in the composites allowing the material to remain amorphous, the partial segregation is observed after the samples are subjected to thermal treatment at 500 °C.

The application of more sophisticated techniques along with FTIR is definitely required, in order to obtain unambiguous data concerning the local atomic arrangement in these composite oxides. The XPS elemental analysis (Table 3) shows that the surface has a different Si:Ti molar composition than the bulk of the composites measured by EDS method. Instead of a nearly equimolar composition measured by EDS, XPS shows Si:Ti molar ratio of 6.2 and 4.4 for Me-500 and Pr-500, respectively. In other words, the surface of the composite is richer in silicon for the smaller particles. Also, the XPS O1s spectra allow assigning oxygen to different oxide species such as Si–O–Si, Ti–O–Ti and Si–O–Ti. The XPS O1s spectra of Me-500 and Pr-500 samples (Fig. 6) show the maximum centered at 532.2 and 532.0 eV, respectively, which corresponds to oxygen of the Si–O–Ti bonds [10]. Though, the peak with the maximum near 532 eV dominates in the spectra of both samples, the deconvolution into Gaussians components reveals that there are two additional significant contributions to the profile, assigned to oxygen of the Ti–O–Ti and Si–O–Si linkages. Thus, the XPS analysis confirms that structure of the composites could be represented mainly as a major homogeneous mixture of the two oxides with a minor content of the segregated SiO_2 and TiO_2.

3.5. TEM observations

Fig. 7a–d shows representative TEM images for Me-500 and Pr-500 samples. The morphology of the particles is completely spherical in both cases but with variable diameter. In addition, the particles in the case of Pr-500 have relatively bigger size than the particles obtained in the case of Me-500. From the particle size histogram of each sample (Fig. 8), we have estimated the average value of particle diameter. These values increase from 70 nm to 420 nm for Me-500 and Pr-500, respectively. The first inspections of both Me-500 and Pr-500 samples, by selected area electron diffraction (SAED) patterns (inset in Fig.7a,b), show that the particles are amorphous. However, HRTEM images (Fig. 7e,f) reveal the presence of nanocrystallites, with diameter of *ca.* 2–4 nm and interplanar distances of *ca.* 2 Å, embedded in the amorphous SiO_2/TiO_2 matrix, which probably correspond to TiO_2 phase. Subsequently, Me-500 and Pr-500 have been examined by STEM-EDS, including qualitative mapping (Fig. 9) and quantitative point analyses. This study reveals the homogenous and uniform distribution of Si and Ti in each individual spherical particle without any apparent preferential concentration in some areas. The average Si/Ti molar ratio (Si:Ti) is *ca.* 1:1. Thus, the TEM study is in good agreement with the spectroscopic investigation, as it makes evident the highly homogeneous distribution of the two oxides in the spheres, but also reveals the presence of small quantity of segregated TiO_2 nanocrystals, which has been proposed on the basis of the XPS and FTIR data.

4. Conclusion

We have demonstrated that application of the combined Stober process and peroxo-mediated solvent-exchange technique results in the formation of nonporous silica–titania spherical particles. The essence of this method is the reaction of the basic solution of aqueous titanium peroxo complex with the TEOS solution in aliphatic alcohols. The choice of a solvent determines the sizes of the SiO_2–TiO_2 spheres; the extended carbon chain of alcohol promotes formation of larger particles with the mean size of 400 nm (in the case of n-propanol), while only 50 nm sized silica–titania composite is obtained if methanol is used. The molecular homogeneity of the composites, in terms of the presence of Si–O–Ti heterolinkages, has been studied by spectroscopic techniques. It has been established that the as-prepared composites show no signs of segregation. After calcination up to 500 °C they stay amorphous due to the stability of the Si–O–Ti bonds in their structure, however, partial

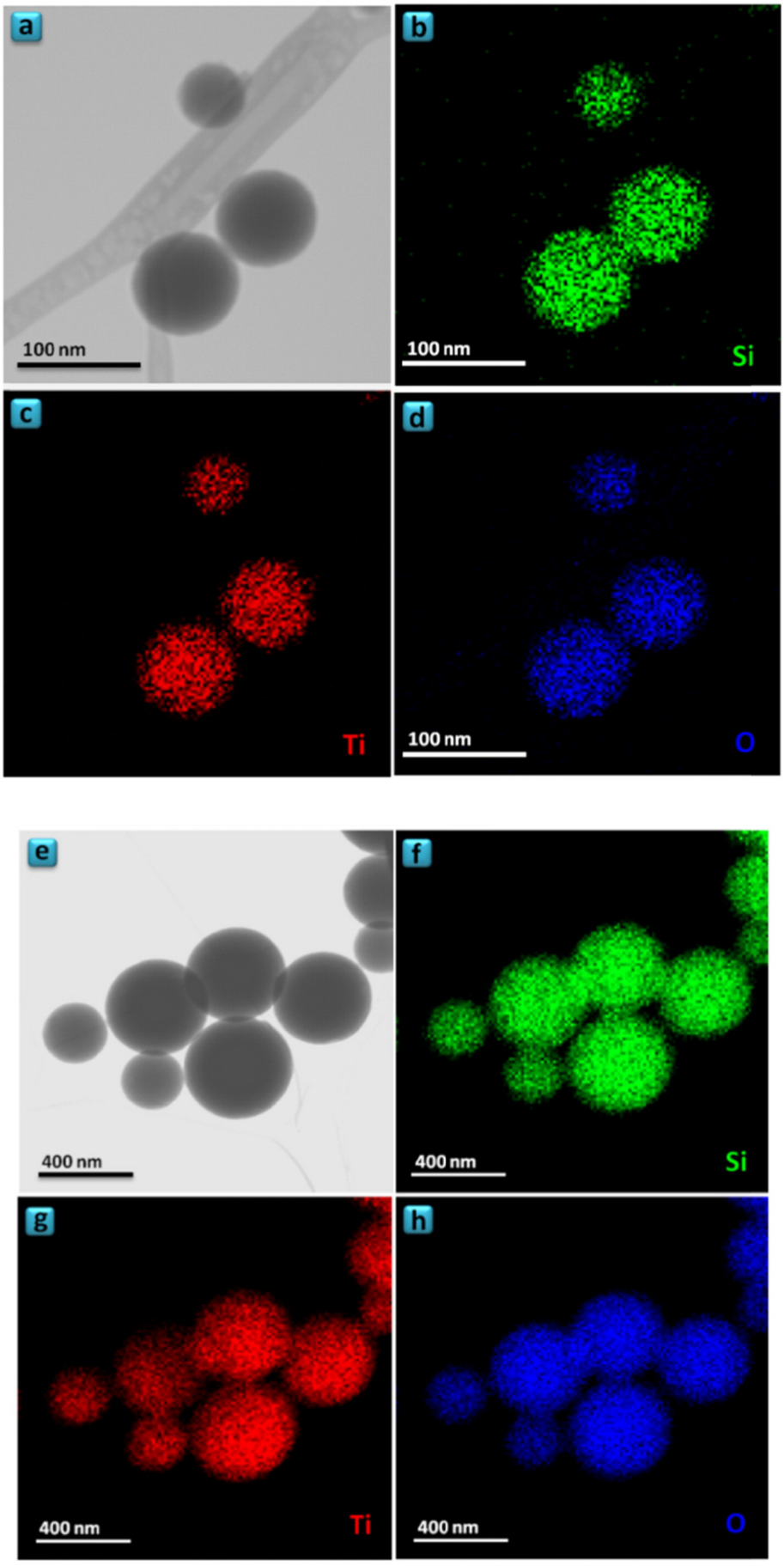

Fig. 9. Elemental mapping for Me-500(a-d) and Pr-500(e-h) particles: (a,e) Bright field-STEM images, (b,f) Si-K$\alpha_1$map, (c,g) Ti-Kα_1 map and (d,h) O-Kα_1 map.

segregation of the two oxides is evident by FTIR, XPS and HRTEM methods. The thermal treatment at higher temperatures leads to the crystallization of TiO_2, with the formation of nanosized anatase crystals at 700 °C and a mixture of anatase and rutile phases at 1000 °C. The described synthetic method is facile and it benefits from the absence of templates or structure-directing agents. The materials prepared *via* the proposed method are of interest for catalytic, photocatalytic and chromatographic applications.

Acknowledgment

South Ural State University is grateful for financial support of the Ministry of Education and Science of the Russian Federation (grant No 16.2674.2014/K). University of Oviedo gratefully acknowledges financial support from the MINECO (MAT2013-40950-R) and FEDER-FICyT (GRUPIN14-060). IK thanks for the support the Russian Foundation for Basic Research 13-03-12188-ofi.

Appendix A. Supplementary data

Supplementary data to this article can be found online at http://dx.doi.org/10.1016/j.jnoncrysol.2015.12.024.

References

[1] X.M. Song, J.M. Wu, G.-J. Zhang, M. Yan, A dual-Layer titania film with enhanced photocatalytic activity, J. Phys. Chem. C 113 (2009) 10681–10688.
[2] L. Sang, Y. Zhao, C. Burda, TiO_2 nanoparticles as functional building blocks, Chem. Rev. 114 (2014) 9283–9318.
[3] A. Kubacka, M. Fernández-García, G. Colon, Advanced nanoarchitectures for solar photocatalytic applications, Chem. Rev. 112 (2012) 1555–1614.
[4] D. Fattakhova-Rohlfing, A. Zaleska, T. Bein, Three-dimensional titanium dioxide nanomaterials, Chem. Rev. 114 (2014) 9487–9558.
[5] M. Cargnello, T.R. Gordon, C.B. Murray, Solution-phase synthesis of titanium dioxide nanoparticles and nanocrystals, Chem. Rev. 114 (2014) 9319–9345.
[6] M. Dahl, Y. Liu, Y. Yin, Composite titanium dioxide nanomaterials, Chem. Rev. 114 (2014) 9853–9889.
[7] Y. Ma, X. Wang, Y. Jia, X. Chem, H. Han, C. Li, Titanium dioxide-based nanomaterials for photocatalytic fuel generations, Chem. Rev. 114 (2014) 9987–10043.
[8] Y. Bai, I. Mora-Seró, F. de Angelis, J. Bisquert, P. Wang, Titanium dioxide nanomaterials for photovoltaic applications, Chem. Rev. 114 (2014) 10095–10130.
[9] S. Klein, S. Thorimbert, W.F. Maier, Amorphous microporous titania–silica mixed oxides: preparation, characterization, and catalytic redox properties, J. Catal. 163 (1996) 476–488.
[10] H.S. Kibombo, R. Peng, S. Rasalingam, R.T. Koodali, Versatility of heterogeneous photocatalysis: synthetic methodologies epitomizing the role of silica support in TiO_2 based mixed oxides, Catal. Sci. Technol. 2 (2012) 1737–1766.
[11] R.J. Davis, Z. Liu, Titania—silica: a model binary oxide catalyst system, Chem. Mater. 9 (1997) 2311–2324.
[12] A. Li, Y. Jin, D. Muggli, D.T. Pierce, H. Aranwela, G.K. Marasinghe, T. Knutson, G. Brockman, J.X. Zhao, Nanoscale effect of silica particle supports on the formation and properties of TiO_2 nanocatalysts, Nanoscale 5 (2013) 5854–5862.
[13] L.J. Alemany, M.A. Bañares, E. Pardo, F. Martín, M. Galán-Fereres, J.M. Blasco, Photodegradation of phenol in water using silica-supported titania catalysts, Appl. Catal. B 13 (1997) 289–297.
[14] S.B. Abd Hamid, S.M. Azad Hossain, M. Eaqub Ali, Silica supported mesoporous titania: a green catalyst for removing environmental pollutants and generating green energy, Adv. Mater. Res. 925 (2014) 694–698.
[15] S. Rasalingam, R. Peng, R.T. Koodali, Removal of hazardous pollutants from wastewaters: applications of TiO_2–SiO_2 mixed oxide materials, J. Nanomater. 617405 (2014).
[16] D.H. Ryu, S.C. Kim, S.M. Koo, D.P. Kim, Deposition of titania nanoparticles on spherical silica, J. Sol-Gel Sci. Technol. 26 (2003) 489–493.
[17] S. Kamaruddin, D. Stephan, The Preparation of silica–titania core–shell particles and their impact as an alternative material to pure nano-titania photocatalysts, Catal. Today 161 (2011) 53–58.
[18] A.F. Demirors, A. van Blaaderen, A. Imhof, Synthesis of eccentric titania–silica core–shell and composite particles, Chem. Mater. 21 (2009) 979–984.
[19] K. Watanabe, D. Nagao, H. Ishii, M. Konno, Rattle-type colloidal crystals composed of spherical hollow particles containing an anisotropic, movable core, Langmuir 31 (2015) 5306–5310.
[20] N. Seriani, C. Pinilla, S. Cereda, A. de Vita, S. Scandolo, Titania—silica interfaces, J. Phys. Chem. C 116 (2012) 11062–11067.
[21] K. Miyashita, S. Kuroda, T. Sumita, T. Ubukata, H. Kubota, Spectrum response of the vacuum-deposited SiO_2/TiO_2 multilayer film with improved photocatalytic activity, J. Mater. Sci. Lett. 20 (2001) 2137–2140.
[22] I. Krivtsov, M. Ilkaeva, V. Avdin, S. Khainakov, J.R. García, S. Ordóñez, E. Díaz, L. Faba, A hydrothermal peroxo method for preparation of highly crystalline silica–Titania photocatalysts, J. Colloid Interface Sci. 444 (2015) 87–96.
[23] M. Andrianainarivelo, R. Corriu, D. Leclercq, P.H. Mutin, A. Vioux, Mixed oxides SiO_2–ZrO_2 and SiO_2–TiO_2 by a non-hydrolytic sol–gel route, J. Mater. Chem. 6 (1996) 1665–1671.
[24] R. Hutter, T. Mallat, A. Baiker, Titania-silica mixed oxides: III. Epoxidation of α-isophorone with hydroperoxides, J. Catal. 157 (1995) 665–675.
[25] M.P. Coles, C.G. Lugmair, K.W. Terry, T.D. Tilley, Titania-silica materials from the molecular precursor $Ti[OSi(OtBu)_3]_4$: selective epoxidation catalysts, Chem. Mater. 12 (2000) 122–131.
[26] B.-S. Lee, D.-J. Kang, S.-G. Kim, Properties of binary TiO_2–SiO_2 composite particles with various structures prepared by vapor phase hydrolysis, J. Mater. Sci. 38 (2003) 3545–3552.
[27] G.N. Shao, R. Sheikh, A. Hilonga, J.E. Lee, Y.-H. Park, H.T. Kim, Biodiesel production by sulfated mesoporous titania–silica catalysts synthesized by the sol–gel process from less expensive precursors, Chem. Eng. J. 215-216 (2013) 600–607.
[28] M. Hirano, K. Ota, H. Iwata, Direct formation of anatase (TiO_2)/Silica (SiO_2) composite nanoparticles with high phase stability of 1300 °C from acidic solution by hydrolysis under hydrothermal condition, Chem. Mater. 16 (2004) 3725–3732.
[29] S. Flaig, J. Akbarzadeh, P. Dolcet, S. Gross, H. Peterlik, N. Hüsing, Hierarchically organized silica–titania monoliths prepared under purely aqueous conditions, Chem. Eur. J. 20 (2014) 17409–17419.
[30] E.I. Morosanova, Silica and silica–titania sol–gel Materials: synthesis and analytical application, Talanta 102 (2012) 114–122.
[31] W. Rupp, N. Husing, U. Schubert, Preparation of silica–titania xerogels and aerogels by sol–gel processing of new single-source precursors, J. Mater. Chem. 12 (2002) 2594–2596.
[32] Z.Y. Wu, Y.F. Tao, Z. Lin, L. Liu, X.X. Fan, Y. Wang, Hydrothermal synthesis and morphological evolution of mesoporous titania—silica, J. Phys. Chem. C 113 (2009) 20335–20348.
[33] B. Mahltig, E. Gutmann, D.C. Meyer, Solvothermal preparation of nanocrystalline anatase containing TiO_2 and TiO_2/SiO_2 coating agents for application of photocatalytic treatments, Mater. Chem. Phys. 127 (2011) 285–291.
[34] W. Chen, Z. Ma, X. Pan, Z. Hu, G. Dong, S. Zhou, M. Peng, J. Qiu, Core@dual-shell nanoporous SiO_2–TiO_2 composite fibers with high flexibility and its photocatalytic activity, J. Am. Ceram. Soc. 97 (2014) 1944–1951.
[35] W. Zhao, L. Feng, R. Yang, J. Zheng, X. Li, Synthesis, characterization, and photocatalytic properties of Ag modified hollow SiO_2/TiO_2 hybrid microspheres, Appl. Catal. B Environ. 103 (2011) 181–189.
[36] M.R. Buchmeiser, New synthetic ways for the preparation of high-performance liquid chromatography supports, J. Chromatogr. A 918 (2001) 233–266.
[37] E.M. Borges, Silica, hybrid silica, hydride silica and non-silica stationary phases for liquid chromatography, J. Chromatogr. Sci. (2014) 1–18.
[38] K. Matsuura, T. Ohmori, M. Nakamura, Y. Itoh, K. Hirano, A simple and rapid determination of valproic acid in human plasma using a non-porous silica column and liquid chromatography with tandem mass spectrometric detection, Biomed. Chromatogr. 22 (2008) 387–393.
[39] M. Karimi, I. Chaudhuryc, C. Jianjunc, M. Safari, R. Sadeghi, M. Habibi-Rezaei, J. Kokini, Immobilization of endo-inulinase on non-porous amino functionalized silica nanoparticles, J. Mol. Catal. B Enzym. 104 (2014) 48–55.
[40] S.J. Soenen, B. Manshian, S.H. Doak, S.C. De Smedt, K. Braeckmans, Fluorescent non-porous silica nanoparticles for long-term cell monitoring: cytotoxicity and particle functionality, Acta Biomater. 9 (2013) 9183–9193.
[41] J.H. Pan, Q. Wang, D. Bahnemann, Hydrous TiO_2 spheres: an excellent platform for the rational design of mesoporous anatase spheres for photoelectrochemical applications, Catal. Today 230 (2014) 197–204.
[42] D. Chen, R.A. Caruso, Recent progress in the synthesis of spherical titania nanostructures and their applications adv, Funct. Mater. 23 (2013) 1356–1374.
[43] C. Oh, J.-H. Lee, Y.-G. Lee, Y.-H. Lee, J.-W. K, H.-H. Kang, S.-G. Oh, New approach to the immobilization of glucose oxidase on non-porous silica microspheres functionalized by (3-aminopropyl)trimethoxysilane (APTMS), Colloids Surf. B 53 (2006) 225–232.
[44] L. Tang, J. Cheng, Nonporous silica nanoparticles for nanomedicine application, Nano Today 8 (2013) 290–312.
[45] Q. Qu, Q. Gu, Z. Gu, Y. Shen, C. Wang, X. Hu, Efficient removal of heavy metal from aqueous solution by sulfonic acid functionalized nonporous silica Microspheres, Colloids Surf. A 415 (2012) 41–46.
[46] D.C.M. Dutoit, M. Schneider, A. Baiker, Titania–silica mixed oxides: I. Influence of sol–gel and drying conditions on structural properties, J. Catal. 153 (1995) 165–176.
[47] S. Yoda, D.J. Suh, T. Sato, Synthesis and characterization of superhydrophobic silica and silica/titania aerogels by sol–gel method at ambient pressure, J. Sol-Gel Sci. Technol. 22 (2001) 75–81.
[48] K. Brodzik, J. Walendziewski, M. Stolarski, L. Van Ginneken, K. Elst, V. Mey-nen, The influence of preparation method on the physicochemical properties of titania–silica aerogels, J. Porous. Mater. 14 (2007) 219–226.
[49] M. Ilkaeva, I. Krivtsov, V. Avdin, S.A. Khainakov, J.R. García, Comparative study of structural features and thermal behavior of mixed silica–titania xerogels prepared *via* the peroxo method and the conventional co-precipitation technique, Colloids Surf. A 456 (2014) 120–128.
[50] W. Stober, A. Fink, E. Bohn, Controlled growth of monodisperse silica spheres in the micron size range, J. Colloid Interface Sci. 26 (1968) 62–69.
[51] I. Krivtsov, M. Ilkaeva, V. Avdin, Z. Amghouz, S. Khainakov, J.R. García, E. Díaz, S. Ordóñez, Exceptional thermal stability of undoped anatase TiO_2 photocatalysts prepared by a solvent-exchange method, RSC Adv. 5 (2015) 36634–36641.
[52] P. Innocenzi, Infrared spectroscopy of sol–gel derived silica-based films: a spectra-microstructure overview, J. Non-Cryst. Solids 316 (2003) 309–319.